Ultramicroscopy 276 (2025) 114200

Contents lists available at ScienceDirect

Ultramicroscopy

journal homepage: www.elsevier.com/locate/ultramic

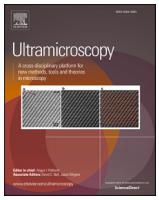

Improving the elemental and imaging accuracy in atom probe tomography of (Ti,Si)N single and multilayer coatings using isotopic substitution of N

Saeideh Naghdali [a,*], Maximilian Schiester [b], Helene Waldl [b], Velislava Terziyska [a], Marcus Hans [c], Daniel Primetzhofer [d], Nina Schalk [a,b], Michael Tkadletz [a]

[a] Department of Materials Science, Montanuniversität Leoben, Franz Josef-Straße 18, 8700 Leoben, Austria
[b] Christian Doppler Laboratory for Advanced Coated Cutting Tools at the Department of Materials Science, Montanuniversität Leoben, Franz Josef-Straße 18, 8700 Leoben, Austria
[c] Materials Chemistry, RWTH Aachen University, Kopernikusstraße 10, 52074 Aachen, Germany
[d] Department of Physics and Astronomy, Uppsala University, Lägerhyddsvägen 1, 75120 Uppsala, Sweden

ARTICLE INFO

Key words:
Atom probe tomography (APT)
Mass spectral overlap
Isotopic substitution
Imaging accuracy
Elemental accuracy
Ti-Si-N

ABSTRACT

This study addresses the challenges in analyzing (Ti,Si)N coatings using atom probe tomography (APT). Overlapping mass-to-charge state ratios in APT mass spectra hinder unambiguous identification of Si and N, thus, isotopic substitution of naturally abundant nitrogen by ^{15}N-enriched nitrogen was applied to disentangle the mass-spectral overlaps. A series of model coatings, namely, Ti-N, Si-N, and Ti-Si-N single layer coatings were utilized to investigate elemental accuracy, while their corresponding multilayer coatings were used to assess lateral resolution and imaging accuracy. The coatings were sputter-deposited using i) naturally abundant nitrogen and ii) ^{15}N-enriched nitrogen, respectively. Subsequently, the coatings were analyzed with a LEAP 5000 XR atom probe. Accuracy in obtained concentrations was cross-validated with elastic recoil detection analysis (ERDA) combined with Rutherford backscattering spectrometry (RBS). The investigation showed that isotopic substitution allows to differentiate the Si and N peaks in the mass spectra and significantly reduces compositional discrepancies between APT and ERDA/RBS results. Despite remaining minor peak overlaps, which can result in inaccuracies in determining the elemental composition, isotopic substitution has proven to be an effective method for peak differentiation and correcting the obtained elemental composition of Ti-Si-N. Moreover, isotopic substitution can predominantly increase the elemental accuracy and imaging accuracy of APT measurements of multilayer coatings.

1. Introduction

Ever-growing demands for prolonging the lifetime and improving the performance of cutting tools require a variety of materials, architectures, and microstructures to make coating design concepts more efficient. Suitable approaches to further enhance the coating properties are based on alloying [1], the formation of (nano)composites [2,3], compositional gradients [4] and multi-/nanolayers [5–7]. Since the mid 1960s, TiN has been used in the cutting industry due to its relatively high hardness and wear resistance [8,9]. However, TiN oxidizes at temperatures higher than 500 °C [10]. The addition of Si to TiN is reported to result either in the formation of a TiSiN solid solution [11] or a nanocomposite structure, consisting of face-centered cubic (fcc) Ti(Si)N nanocrystals embedded in an amorphous SiN_x tissue phase [12]. This nanocomposite microstructure allows hardness values of ~50 GPa [13], as well as high wear resistance and oxidation stability above 800 °C [14]. However, the detailed characterization of nanocomposite TiSiN coatings remains challenging. Typically X-ray photoelectron spectroscopy (XPS) would be a suitable method to detect amorphous phase fractions, but in the present case the close binding energies of crystalline (100.6 eV) [15] and amorphous SiN_x (101.8 eV) [16] make a differentiation difficult. In addition, the possibility of solid solution formation on one hand and the typically low thickness of the amorphous tissue phase (down to 1-2 monolayers according to Vepřek et al. [13]) on the other hand, challenge the investigation of the local Si distribution using high resolution transmission electron microscopy (HR-TEM) [14].

Thus, atom probe tomography (APT) would be the method of choice to study the local distribution of Si with a resolution close to atomic

* Corresponding author.
E-mail address: saeideh.naghdali@unileoben.ac.at (S. Naghdali).

https://doi.org/10.1016/j.ultramic.2025.114200
Received 21 January 2025; Received in revised form 10 June 2025; Accepted 16 June 2025
Available online 17 June 2025

scale. Tang et al. [17] investigated Ti-Si-N coatings using pulsed laser APT and reported that segregation of Si at the grain boundaries could not be detected, however, they concluded that there still remains the possibility of the presence of thin amorphous layers, which could not be resolved due to trajectory aberrations, event multiplicity and last but not least, overlap of mass-to-charge state ratios in the mass spectra. For example $^{14}N^{+}$ and $^{28}Si^{2+}$ [18] are detected at similar mass-to-charge state ratios (14.00 and 13.99 Da, respectively), which results in significant errors in the quantitative determination of the elemental composition and a low imaging accuracy and precision. Imaging accuracy refers to the obtained spatial position of detected species within 3D reconstructions with respect to the true position in the evaporated specimen. Imaging precision refers to the repeatability of the determined atomic positions across multiple evaluations. However, since the imaging precision can still be high, if the evaluation is consistent, but the imaging accuracy is strongly affected by peak overlaps, we refer in the following to the imaging accuracy. London et al. [19] demonstrated that applying a single-ion deconvolution technique can effectively resolve overlapping peak even with spatial resolution. They noted, however, that the technique is most effective when the overlapping ions originate from different regions of the specimen — i.e., spatial variations exist. As this is not the case within the individual layers of the coatings examined in this study, this method is not applicable. Kinno et al. [20] showed that using isotopic ^{15}N for the synthesis of SiN allows to resolve the peak overlaps of the main isotopes in the APT mass spectrum and thus enables qualitative and quantitative analysis of the nitrogen distribution. Engberg et al. [18,21] demonstrated that isotopic substitution of naturally abundant nitrogen with ^{15}N enables quantitative differentiation of Si and N in APT of Ti-Si-N coatings, achieving good agreement with elastic recoil detection analysis (ERDA). They further visualized nanometer-scale Si compositional fluctuations using voxelized data and confirmed, via TEM, the segregation of Si on nanometer scale, potentially around TiN. However, it was concluded that the studied cathodic arc-deposited coatings were nanostructured rather than nanocomposite, as no strongly developed SiN tissue phase was observed. Several studies [22–24] have reported the formation of either solid solution or nanocomposite structures in sputter deposited TiSiN coatings. However, none of these studies have employed APT.

Thus, while works on APT of cathodic arc deposited Ti-Si-N coatings using isotopic substitution of naturally abundant nitrogen with ^{15}N-enriched nitrogen are available, no literature on sputter deposited Ti-Si-N coatings is available. In order to close this gap, well defined single and multi-layer model coatings were applied. This approach not only allows to evaluate the improvement in quantitative determination of the elemental composition, but also provides a measure for the improvement in spatial accuracy and differentiation of different ion species within the 3D reconstruction. Therefore, the present work evaluates the feasibility of isotopic substitution of nitrogen using sputter-deposited model single and multilayer coatings with the ultimate goal to investigate the local elemental distribution in Ti-Si-N nanocomposite coatings employing APT. Ti-Si-N, Si-N and Ti-N single layer coatings as well as Ti-N/Si-N, Ti-Si-N/Si-N, and Ti-N/Ti-Si-N multilayer coatings were sputtered using both, naturally abundant and ^{15}N-enriched nitrogen and subsequently investigated by APT. This methodology allows to highlight the effectiveness of isotopic substitution to differentiate the peak overlaps and, therefore, to gain insight into spatially resolved elemental distribution of (Ti,Si)N coatings. The elemental compositions are compared to reference compositions gained by ERDA combined with Rutherford backscattering spectrometry (RBS).

2. Material and methods

2.1. Coating deposition

Prior to the deposition, Si substrates with dimensions of 7×21 mm^2 were ultra-sonically cleaned in acetone and ethanol. The substrates were mounted in a laboratory scale unbalanced d.c. magnetron sputter deposition system, equipped with one Si (99.99 %) and two Ti (99.995 %) targets (ø 2 in) with target to substrate distance of 45 mm. The deposition system was evacuated to a pressure $<10^{-4}$ Pa and the substrates were heated up to 700 °C. Subsequently, the substrates were cleaned in an Ar^{+} ion etching process at a frequency of 50 kHz using a voltage of −500 V for 10 min. Reactive deposition of Si-N, Ti-N, Ti-Si-N coatings was done in a mixed Ar/N_2 atmosphere at a working pressure of 0.42 Pa (the N_2 partial pressure was 0.04 Pa). Two sets of coatings were deposited; one using naturally abundant and one using ^{15}N-enriched nitrogen, specifically a N-enriched gas containing 98 at% ^{15}N purchased from Sigma-Aldrich. The constant target currents were set to 0.10 A and 0.35 A for Si and Ti, respectively. During deposition of Ti-N, a bias voltage of −50 V was applied, while the other coatings were synthesized at floating potential. The total deposition time was 150 min, resulting in coating thicknesses of ~1.5-2 μm. The same deposition system was employed to deposit multilayer coatings comprising alternating layers, each designed to have individual layer thicknesses of ~10 nm. In this process, computer-controlled shutters were utilized to control the layer thickness and composition. A 500 nm sacrificial Ti-N capping layer was also synthesized on top of the multilayer coatings in order to facilitate the preparation of atom probe specimens by focused ion beam (FIB) during final sharpening. Detailed deposition parameters and total thicknesses as measured by scanning electron microscopy (SEM) are summarized in Table 1.

2.2. Coating characterization

Imaging of the cross-sections of the coatings was done using a Zeiss GeminiSEM 450 SEM. A Hitachi IM4000+ ion milling system was applied to prepare the cross-sections. The reference composition of the single layer coatings was determined by complementary ion beam based techniques utilizing the 5MV Pelletron tandem accelerator at the Tandem Laboratory of Uppsala University [25]. ERDA and RBS, using 36 MeV I^{8+} and 2 MeV He^{+} primary ions, respectively, were employed and a stoichiometric TiN reference sample was used [26]. The total measurement uncertainty was 3 % relative from the deduced values and further details are available in [27]. In order to gain information about the local elemental composition, the coatings were investigated by laser-assisted APT (CAMECA LEAP 5000 XR) with an ultraviolet laser (355 nm wavelength). Waldl et al. [28] showed that significant loss of N is observed at laser pulse energies above 30 pJ using UV lasers. Thus, in the current study, the laser pulse energy was set to 30 pJ. The laser pulse frequency, base temperature, and detection rate were kept at 250 kHz, 50 K, and 0.5 %, respectively. The specimens for the APT measurements were prepared using a 3D-Micromac microPREP PRO FEMTO laser micromachining system with subsequent FIB annular milling using a FEI Versa 3D dual beam workstation. More details on the preparation of the specimens can be found in ref [29]. Evaluation of APT data was done using the IVAS module within the AP Suite 6.3.0 software package. Identifying the position of the maximum intensity of each peak and corresponding peak onset from the background was used in ranging of the mass spectra. More details about the ranging can be found in ref

Table 1
Deposition parameters of investigated coating systems and thickness measured by SEM.

Coating	Target current [A]			Thickness [μm]
	Si	**Ti**	**Ti**	
Si-N	0.2	-	-	~1.70
Ti-N	-	0.35	0.35	~1.88
Ti-Si-N	0.1	-	0.35	~2.05
Ti-N/Si-N	0.2	0.35	0.35	~1.40
Ti-N/Ti-Si-N	0.1	0.35	0.35	~1.58
Ti-Si-N/Si-N	0.1	-	0.35	~1.25

[30]. For the multilayered coatings, iso-concentration surfaces were used to define the individual layer limits and interface zone, while individual layers were exported as a separate data set from the volume enclosed by iso-concentration surfaces and investigated individually. Subsequently, the mass spectra of the individual data sets were analyzed, and the elemental compositions were evaluated and compared with the corresponding single layer coatings as well as reference compositions.

3. Results and discussion

3.1. Microstructure of the coatings

Fig. 1 displays cross-sectional SEM images of the single layer coatings (a-c) and multilayer coatings (d-f) deposited on Si substrates using naturally abundant nitrogen. As all deposition parameters were kept constant, independent of the nitrogen supply, the total thicknesses and cross-sectional morphologies of corresponding coatings synthesized using ^{15}N-enriched nitrogen are comparable and shown in Figure S1 in the supplementary material. As visible in Fig. 1a, the Si-N coating shows a featureless cross-section, indicating an amorphous or very fine-grained structure. In contrast, the Ti-N coating in Fig. 1b exhibits columnar grains, highlighting the crystalline structure. The Ti-Si-N coating in Fig. 1c shows again a featureless cross-section, indicating that the addition of Si to Ti-N results in a significant grain refinement or even the formation of an amorphous phase. The cross-sectional structures of the Ti-N/Si-N and Ti-N/Ti-Si-N multilayers, as illustrated in Fig. 1d and Fig. 1f, reveal a bilayer thickness of ~20 nm, as aimed for. However, in the Ti-Si-N/Si-N multilayer coating, Fig. 1e, the measured thicknesses are ~4 nm for Si-N and ~7 nm for Ti-Si-N. This discrepancy can be attributed to the deposition parameters, specifically the selection of 0.1 A current for the Si target during the deposition of Si-N layers in this multilayer coating system.

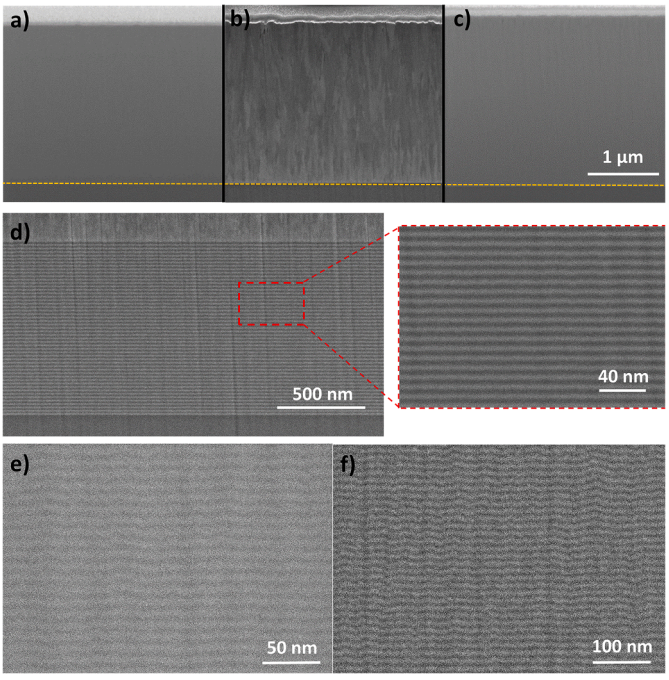

Fig. 1. SEM cross-section images of a) Si-N, b) Ti-N, and c) Ti-Si-N single layer, where the dashed line corresponds to the substrate/coating interface, and d) Ti-N/Si-N e) Ti-Si-N/Si-N, and f) Ti-N/Ti-Si-N multilayer coatings synthesized using naturally abundant nitrogen.

3.2. Limitations of APT for (Ti,Si)N using naturally abundant nitrogen

To investigate the elemental distribution of the (Ti,Si)N single and multilayer coatings, APT was performed. The first evaluation step of APT data involves identification of the peaks present in the mass spectrum. While there are no peak overlaps in the mass spectrum of Ti-N, limitations are present in the mass spectra of Si-N as well as Ti-Si-N. The mass spectrum of the ternary Ti-Si-N single layer coating, deposited using naturally abundant nitrogen containing 2×10^7 ions, is exemplarily shown in Fig. 2a (mass spectra of Ti-N and Si-N single layer coatings are presented in the supplementary material Figure S2 and Figure S3). The mass spectrum consists of elemental species (Si^+, Si^{2+}, N^+, Ti^{2+}, Ti^{3+}) as well as molecular ions (N_2^+, TiN^+, TiN^{2+}, SiN^+, Si_2N^{2+}). The isotopic signatures of Ti and TiN ion species were clearly discernible and exhibited five distinct and well-separated visible peaks in the mass spectrum. However, the peaks at 14, 14.5, 15, 28, 29, and 30 Da are attributable to multiple ion species. These peak overlaps result in noticeable shoulder effects, as shown in Fig. 2b and Fig. 2c. For instance, the peak at 14 Da is attributable to $(^{14}N^{14}N)^{2+}$ and/or $^{14}N^+$ (which could slightly influence the obtained composition [31]) or $^{28}Si^{2+}$ or mixture of them, and the peak at 15 Da to $(^{15}N^{15}N)^{2+}$and/or $^{15}N^+$ or $^{30}Si^{2+}$ or mixture of them. The intensity of the peak at 14.5 Da can serve as an indicator for the presence of either $^{29}Si^{2+}$ or $(^{14}N^{15}N)^{2+}$. Based on Kingham diagrams [32,33], double ionization of N_2 is favored at electric field strengths above 60 V nm^{-1} [34]. The maximum electric field strength estimated from Kingham diagrams in the current study is 37.5 V nm^{-1} (based on the Ti^{3+}/Ti^{2+} charge state ratio)[33], which emphasizes the most probable presence of $^{29}Si^{2+}$peak at 14.5 Da, $^{28}Si^{2+}$and/or $^{14}N^+$ at 14 Da, and $^{30}Si^{2+}$ and/or $^{15}N^+$ at 15 Da. Therefore, the peaks at 28, 29 Da are attributable to couples of $^{28}Si^+$and/or $(^{14}N^{14}N)^+$, $^{29}Si^+$and/or $(^{14}N^{15}N)^+$, respectively. The peak at 30 Da could be attributed to $^{30}Si^+$ or $(^{46}Ti^{14}N)^{2+}$. However, considering naturally abundant isotopic ratios, the peak at 30 Da in Ti-Si-N coating was assigned to $(^{46}Ti^{14}N)^{2+}$. The Si-N coating presents identical peak overlaps with Ti-Si-N, except the peak at 30 Da which could be attributed to $^{30}Si^+$and/or $(^{15}N^{15}N)^+$. Within this study, it was decided to assign multiple species to the aforementioned overlapping peaks, utilizing a rough 50-50 ranging for the coatings grown with naturally abundant nitrogen. It is expected that such assignments result in inaccurate elemental compositions. Indeed, it is obvious that the peak overlaps result in a significant deviation of estimated elemental composition from APT data in the Si-N and Ti-Si-N coatings, deposited with naturally abundant nitrogen, from the reference composition, as summarized in Table 2.

Fig. 3 shows 3D reconstructions of the APT data gained from the Si-N, Ti-N and Ti-Si-N single layer coatings deposited using naturally abundant nitrogen, based on mass spectrum analysis. The ion distribution seems uniform for Si, Ti, and N, however, due to the peak overlaps in the mass spectrum, possible clustering of elements cannot be excluded. While peak decomposition and deconvolution techniques have advanced, they are primarily applied to correct bulk compositions rather than resolve spatial ion distributions, making it challenging to accurately identify spatial elemental fluctuations. Cojocaru-Mirédin et al. [35] demonstrated that APT has the potential to locally characterize chemical bonds by determining the probability of molecular ions (PMI) and the probability of multiple detection events (PME). PMI and PME values of the single layer coatings deposited with naturally abundant nitrogen are added to Fig. 3. Comparing the PME and PMI values with values reported in ref [35] confirms the presence of covalent bonds, as also reported in various other studies [2,21,36,37].

In contrast to Ti-Si-N and Si-N, there are no peak overlaps between Ti and N in the Ti-N mass spectrum, allowing for a more accurate quantification of the elemental composition. Based on the mass-to-charge state ratio, the peak at 30 Da in the Ti-N coating, deposited by naturally abundant nitrogen, could be attributed to $(^{15}N^{15}N)^+/(^{46}Ti^{14}N)^{2+}$. However, considering naturally isotopic abundancies, this peak is assigned to $(^{46}Ti^{14}N)^{2+}$. The elemental composition of Ti and N in the Ti-

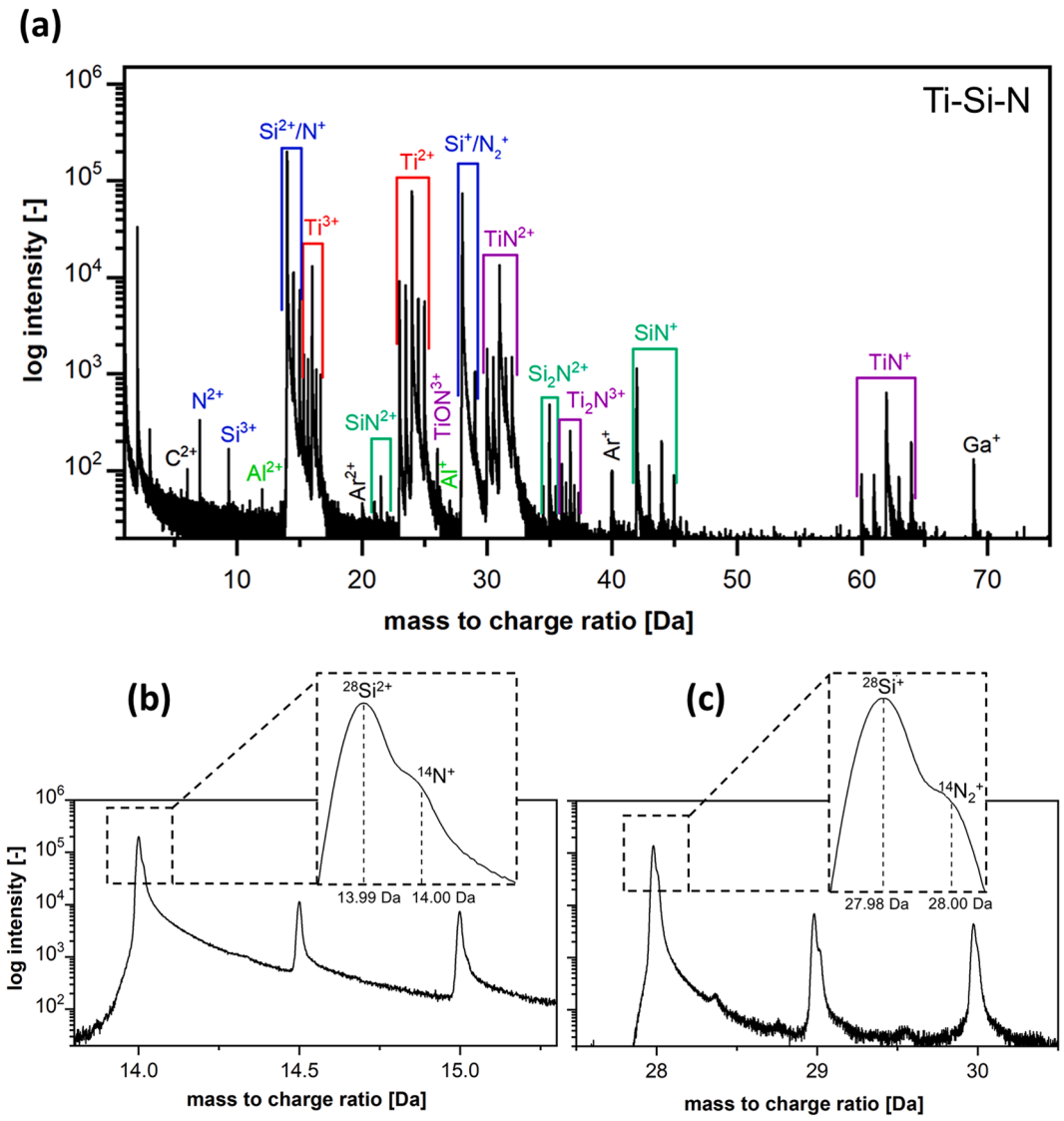

Fig. 2. a) Mass spectrum of Ti-Si-N, deposited with naturally abundant nitrogen. A detailed view of the occurring peak overlaps can be seen in (b) from 13.8 to 14.1 Da and (c) from 27.9 to 28.1 Da.

Table 2
Reference composition of coatings deposited with naturally abundant nitrogen obtained by ERDA/RBS compared to elemental composition determined by APT.

	ERDA/RBS [at%]				APT [at%]			
	Ti	**Si**	**N**	**O**	**Ti**	**Si**	**N**	**O**
Si-N	-	71.4 ±0.8	28.0 ±0.8	0.5 ±0.1	-	47.6	52.3	0.1
Ti-Si-N	21.6 ±0.8	23.3 ±0.9	54.4 ±1.6	0.7 ±0.1	28.5	23.7	47.7	< 0.1
Ti-N	49.9 ±1.5	–	48.5 ±1.5	1.7 ±0.1	51.5	-	47.1	1.4

N coating as shown in Table 2, is in reasonable agreement with the reference composition obtained by ERDA/RBS. However, the nitrogen content is ~2 at% lower than the reference value, which can be related to the dissociation tendency of nitrogen-carrying molecular ions in the atom probe, which produces undetectable neutral fragments, affecting the determined nitrogen content [28,30,34,38]. An indication for this phenomenon can be observed in the presence of Ti_2N^{3+} ion species, as shown in Fig. 3. This species serves as the parent molecule for the

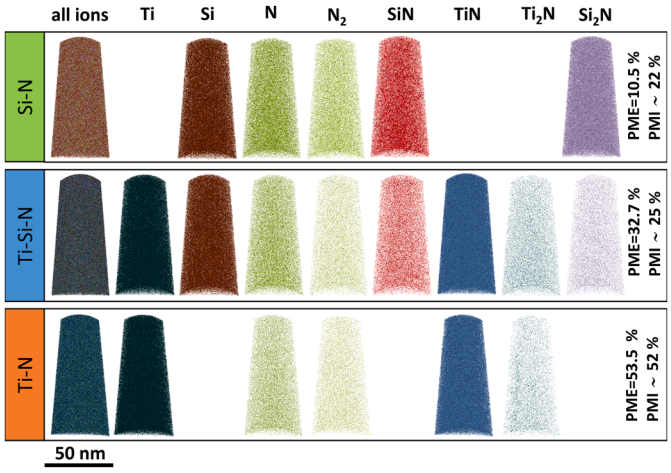

Fig. 3. APT 3D reconstructions of ion distributions in Si-N, Ti-Si-N, and Ti-N single layer coatings, deposited with naturally abundant nitrogen.

dissociation into Ti^{2+} and TiN^{+} ions [39].

3.3. Improving elemental accuracy of (Ti,Si)N by isotopic substitution of nitrogen

Fig. 4 and Figure S4 illustrate that using ^{15}N-enriched nitrogen substituted nitrogen for the deposition of Ti-Si-N and Si-N coatings mostly resolves peak overlaps in the mass spectra, though minor overlaps at 15 and 30 Da remain. Since there are no peak overlaps in the Ti-N mass spectrum, conducting APT measurements on this coating deposited with ^{15}N-enriched nitrogen were omitted. For Si-N and Ti-Si-N coatings, the majority of detected ions in the peaks at 14, 28, and 29 Da corresponds to Si. However, the peak at 15 Da can either be attributed to $^{15}N^{+}$ or $^{30}Si^{2+}$ or mixture of both, and the peak at 30 Da can be attributed to $(^{15}N^{15}N)^{+}$ or $^{30}Si^{+}$ or mixture of both. Taking into account that 98 at% of the gas consists of ^{15}N, the vast majority of ions detected at 15 and 30 Da are most probably ^{15}N ion species. However, the ^{30}Si ion species with an isotopic abundancy of 3.09 % [40] also contributes to these peaks. Therefore, based on isotopic abundancies, the peaks at 15 and 30 Da were assigned to ^{15}N. Due to the isotopic substitution, the first TiN^{2+} peak ($^{46}Ti^{15}N$) shifts to 30.5 Da, resulting in no overlap of TiN^{2+} with $(^{15}N^{15}N)^{+}$ at 30 Da in the Ti-Si-N coating. The elemental composition of the coatings deposited with ^{15}N-enriched nitrogen determined by APT is compared to the reference composition obtained by ERDA/RBS in Table 3. Considering uncertainties of ERDA/RBS data, the Si and N contents in the Si-N coating with ^{15}N-enriched nitrogen obtained by APT show a substantial improvement compared to the coatings deposited with naturally abundant nitrogen. The remaining differences from the reference compositions can be attributed to the minor peak overlaps at 15 and 30 Da. Local compositional variations between the individual

Table 3
Reference elemental composition of coatings, deposited with ^{15}N-enriched nitrogen, obtained by ERDA/RBS compared to composition determined by APT.

	ERDA/RBS [at%]				APT [at%]			
	Ti	**Si**	N	**O**	**Ti**	**Si**	**N**	**O**
Si-N	-	71.8 ±0.8	28.1 ±0.8	0.2 ±0.1	-	79.8	19.4	0.8
Ti-Si-N	24.1 ±0.9	21.7 ±0.8	54.2 ±1.6	< 0.1	25.0	26.4	48.5	< 0.1
Ti-N	49.7 ±1.5	-	50.3 ±1.5	< 0.1	-	-	-	

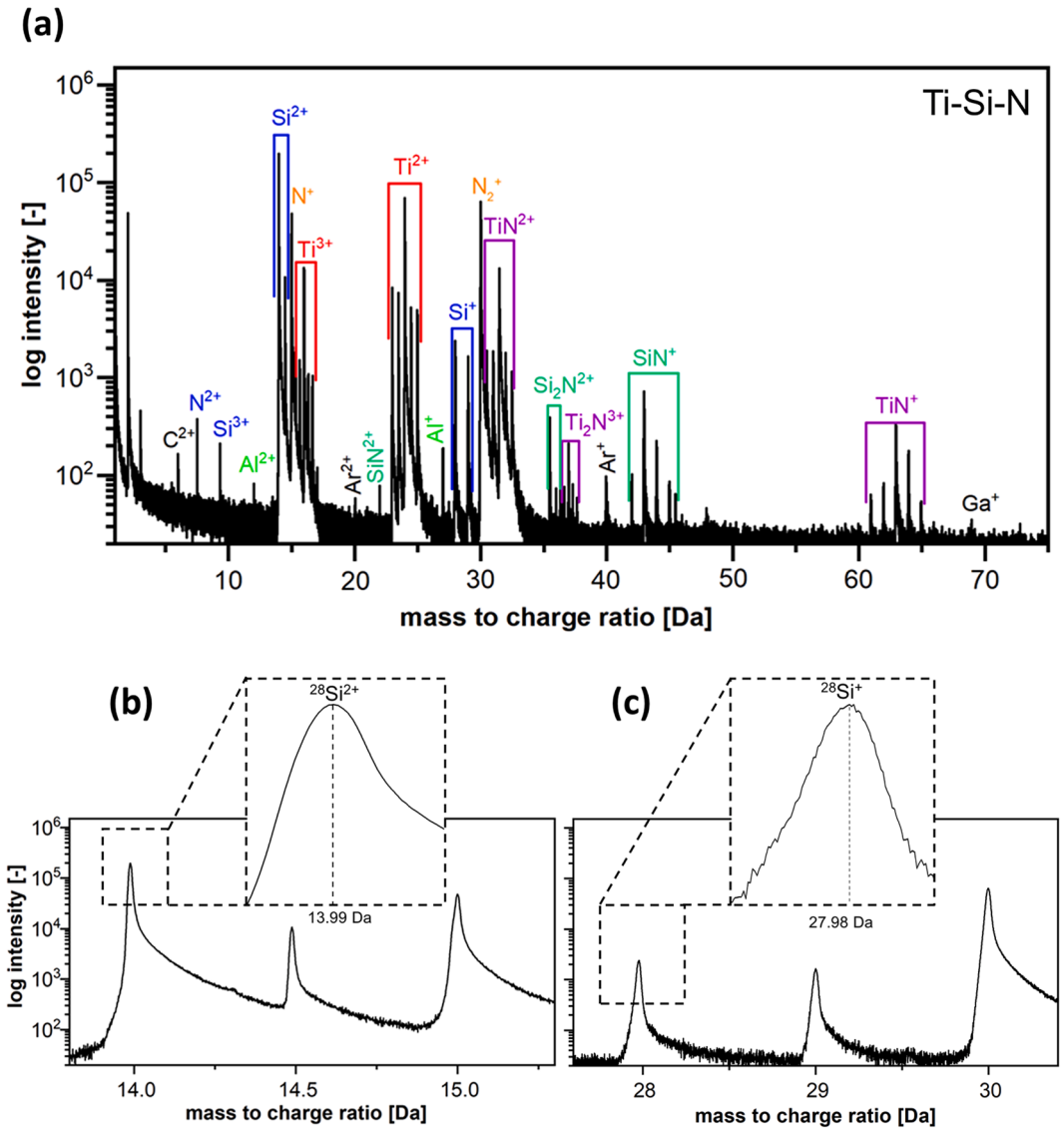

Fig. 4. (a) Mass spectrum of Ti-Si-N, deposited with ^{15}N-enriched nitrogen. A detailed view of the avoided peak overlaps can be seen in (b) and (c).

grains, and, as mentioned before, the detection of multiple events as well as the dissociation of N-containing molecular ions also influence the accuracy of the quantitative compositional analysis [28,30,34,38].

In order to demonstrate the reliability of APT reconstructions in a multilayer system, the Ti-N/Si-N, Ti-N/Ti-Si-N, and Ti-Si-N/Si-N multilayer coatings deposited using both naturally abundant and ^{15}N-enriched nitrogen were studied via APT and are discussed in the following.

3.4. Ti-N/Si-N multilayer system

The 3D APT reconstruction of the Ti-N/Si-N multilayer coating with ^{15}N-enriched nitrogen in Fig. 5a shows alternating individual layers. The reconstruction parameters including initial tip radius and image compression factor were adjusted to obtain a reconstruction where the layer thicknesses fit as close as possible to the results observed via SEM, i.e. ~ 8-10 nm. Due to the fact, that the different layers exhibit different electric field strengths for evaporation, but only one field strength can be specified in the evaluation software, an altered geometry of the reconstruction is observed. As a consequence, the reconstruction will be affected by artifacts, such as density variations [41]. Fig. 5a presents the corresponding 1D compositional profile (Z direction, perpendicular to interface). An abnormal shape is observed for Si at the interface where the Ti-N layer ends and the Si-N layer begins, and similarly for Ti where Si-N ends and Si-N begins. These irregularities might indicate artifacts associated with field evaporation of dissimilar materials [42] particularly when shifting from a high electric field material ($Si_{pure,\ at\ low\ T}$,33 V/nm) to a low electric field material ($Ti_{pure\ at\ low\ T}$, 26 V/nm) [43]. In Fig. 5a, a proximity histogram evaluated throughout the Si-N into the Ti-N layer is shown. For comparison, the reference composition of the corresponding single layers as determined by ERDA/RBS (compare also Table 1) is added to the diagram. A few percent of Si and Ti can be observed in the Ti-N and Si-N layers, respectively. The determination of the exact iso-concentration value is biased due to the occurrence of density fluctuations, a reconstruction artifact, attributed to the varying evaporation field between the individual layers. The corresponding mass spectra of the individual Ti-N and Si-N layers are shown in supplementary materials Figure S5. The peaks at 14,15, 28, 29, and 30 Da in the mass spectrum of Ti-N layers were only attributed to nitrogen ion species. The present peak at 14.5 Da in the Ti-N layers was assigned to $^{29}Si^{2+}$ and therefore results in existence of a few percent of Si in Ti-N layers. Accordingly, elemental composition of Ti-N layers has been estimated 51.4 at% Ti, 47.2 at% N, and 0.2 at% Si. The mass spectrum of the Si-N layers also shows weak Ti and Ti-N peaks. Peaks at 14, 15, 28, 29, and 30 Da were assigned based on same argument as in the corresponding single layer coatings. Accordingly, elemental composition of Si-N layers has been estimated 79.6 at% Si, 18.8 at% N, and 0.9 at% Ti. Besides the presence of a few percent Si in Ti-N and vice versa, which can be related to minor inter-diffusion or/and remaining peak overlaps of minor isotopes, the elemental compositions of both Si-N and Ti-N layers are in a fair agreement with their corresponding single layers and reference composition measured by ERDA/RBS.

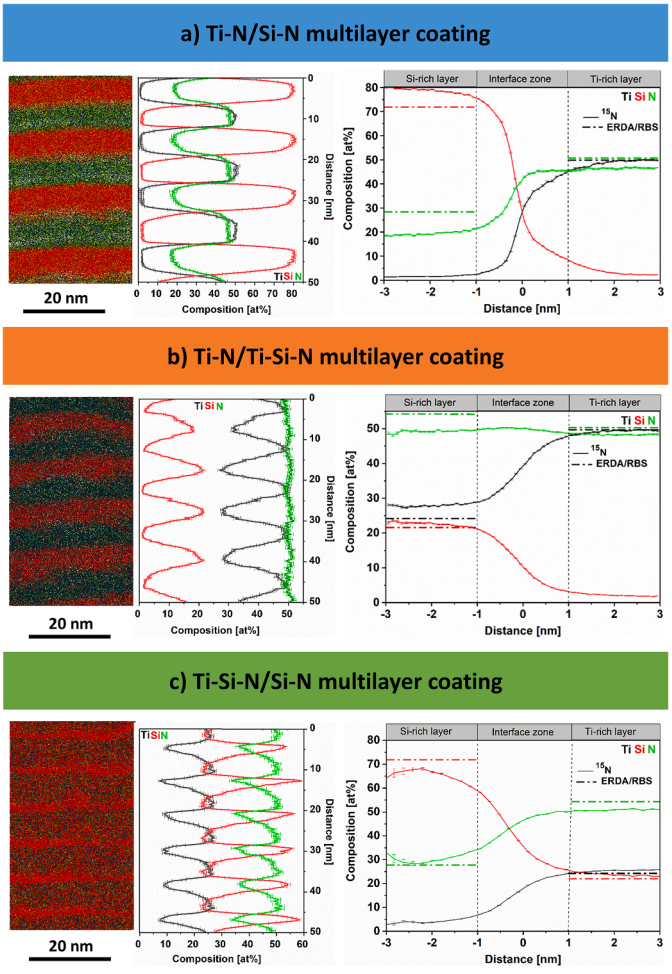

Fig. 5. APT 3D reconstructions, corresponding 1D concentration profiles, and proximity histograms across one interface in multilayer coatings, deposited with ^{15}N-enriched nitrogen.

3.5. Ti-N/Ti-Si-N multilayer coating system

The 3D APT reconstruction and correlating 1D compositional profile of the Ti-N/Ti-Si-N multilayer coating with ^{15}N-enriched nitrogen are illustrated in Fig. 5b. The Ti content in the Ti-Si-N layers is higher than the reference composition of the corresponding single layer measured by ERDA/RBS, which can be also seen in the proximity histogram in Fig. 5b. Because Ti ion species do not share the same mass-to-charge state ratios with other ions, peak overlaps cannot explain this deviation. However, the target setup was different for this multilayer coating (see Table 1), which might influence the coating composition. During the deposition of the Ti-N/Ti-Si-N multilayer coating, always two Ti targets were continuously running. The mass spectra of Ti-N and Ti-Si-N layers are shown in supplementary material Figure S6. As described before, peak assignment has been done according to the naturally isotopic abundancies. Nevertheless, the existence of a peak at 14.5 Da indicates the presence of a few percent Si in Ti-N (49.7 at% Ti, 49.7 at% N, and 0.1 at % Si) layers, which can, analogously to the Ti-N/Si-N multilayer, be related to inter-diffusion during deposition or/and remaining peak overlaps of minor isotopes. The higher Ti content in the Ti-Si-N (29.2 at % Ti, 19.9 at% Si, and 50.6 at% N) layers can, as described above, be related to the different deposition setup, which in turn results in a lower Si and N content compared to the single layer coatings (Table 3). The proximity histogram also demonstrates the efficacy of isotopic substitution in distinguishing layers across the Ti-N/Ti-Si-N interface

3.6. Ti-Si-N/Si-N multilayer coating system

Fig. 5c shows the 3D reconstruction of the Ti-Si-N/Si-N multilayer coating system where a decreased thickness of the Si-N layers is seen, which is in good agreement with the reduced layer thicknesses observed by SEM, Fig. 1e, and is most likely related to the lower current applied to the Si target (0.1 A) compared to the current used in the Si-N single layer coating (0.2 A, compare also Table 1). Fig. 5c shows the 1D compositional profile and proximity histogram of the Ti-Si-N/Si-N multilayer coating system. Unlike the proximity histogram which allows a more accurate assessment [42] of the Si and N content in Si-N layers, yielding values close to the reference composition measured by ERDA/RBS, the 1D compositional profile still shows inaccuracies in estimating the

elemental composition of Si-N layers. Indeed, the 1D concentration profile does not consider the curvature of the interface, resulting in inaccurate statistics and artificially broadening of the interface region [44], which affects the estimated elemental composition of the Si-N layer. Based on the assigned mass spectra in supplementary material Figure S7, the elemental composition of Si-N layers is 59.7 at% Si, 32.8 at% N, and 7.3 at% Ti, while the elemental composition of Ti-Si-N layers is 26.0 at% Ti, 23.2 at% Si, and 50.7 at% N. Lower Si content in Si-N layers compared to the reference composition can be related to present minor peak overlaps of Si and N. The quite high content of additional Ti found in the Si-N layers can be attributed to the rather thin Si-N layers, which may cause inaccuracies in defining iso-surfaces and hinder precise data extraction from the entire dataset.

3.7. Imaging accuracy

Fig. 6 shows a comparison of the 3D reconstructions of Si in the multilayer coatings deposited with naturally abundant and ^{15}N-enriched nitrogen. Si was selected as an indicator to assess the imaging accuracy, because Ti does not exhibit any peak overlaps, and nitrogen is present in all layers. To ensure comparability, for all reconstructions 80 % of the detected Si ions are displayed and a spherical representation with a radius of 0.22 nm has been chosen. It is clearly visible that in the multilayer coatings deposited with naturally abundant nitrogen, the contributions of Si and N can as a result of the peak overlaps not be unambiguously distinguished, reducing the imaging accuracy. However, in the multilayer coatings deposited with ^{15}N-enriched nitrogen, the spatial distribution of Si is clearly improved by differentiating overlapping peaks, demonstrating the effectiveness of isotopic substitution of nitrogen. Nevertheless, the presence of Si in Ti-N layers can be attributed to minor inter-diffusion or/and remaining peak overlaps of Si and N, as previously discussed.

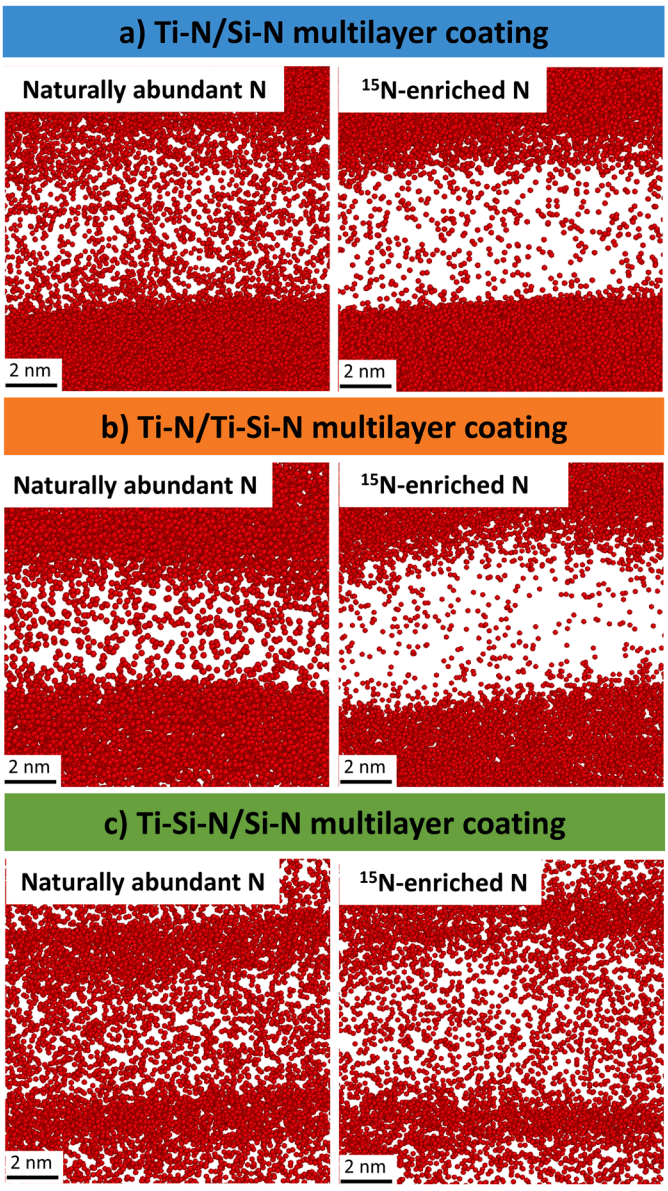

Fig. 6. APT 3D reconstructions of Si (clipped view) in a) Ti-N/Si-N, b) Ti-N/Ti-Si-N, and c) Ti-Si-N/Si-N multilayer coatings deposited with naturally abundant and ^{15}N-enriched nitrogen.

4. Conclusions

We have investigated the effectiveness of isotopic substitution of naturally abundant nitrogen by ^{15}N-enriched nitrogen to differentiate the peak overlaps and therefore enhance the elemental accuracy and imaging accuracy in (Ti,Si)N coatings using APT. Complementary ERDA/RBS data were used as reference compositions. It has been shown that substitution of naturally abundant nitrogen with isotope ^{15}N-rich (98 at%) nitrogen allows to differentiate the Si and N peaks in the mass spectra and significantly decreases compositional discrepancies between APT and ERDA/RBS results. However, still small differences between APT and ERDA/RBS data remain, highlighting the influence of minor peak overlaps of Si and N, multiple detection events and also dissociation tendency of N-carrying molecular ions into neutral fragments, which are not detectable in APT. Using isotopic substitution the local elemental distribution could be predominantly resolved in (Ti,Si)N multilayer coating systems, as demonstrated in the 1D composition profiles and proximity histogram. This practical methodology improves imaging accuracy, thus, facilitating the differentiation of the various layers within the multilayer coatings, which provides the basis for a deeper and more detailed understanding. The present work has established a toolbox using model sputtered coatings to further investigate Ti-Si-N coatings via APT.

CRediT authorship contribution statement

Saeideh Naghdali: Writing – original draft, Visualization, Investigation, Formal analysis, Conceptualization. **Maximilian Schiester:** Writing – review & editing, Investigation, Formal analysis, Conceptualization. **Helene Waldl:** Writing – review & editing, Investigation, Formal analysis. **Velislava Terziyska:** Writing – review & editing, Investigation. **Marcus Hans:** Writing – review & editing, Investigation, Funding acquisition, Formal analysis. **Daniel Primetzhofer:** Writing – review & editing, Investigation, Funding acquisition, Formal analysis. **Nina Schalk:** Writing – review & editing, Supervision, Project administration, Funding acquisition, Conceptualization. **Michael Tkadletz:** Writing – review & editing, Supervision, Project administration, Methodology, Funding acquisition, Conceptualization.

Declaration of competing interest

The authors declare that they have no known competing financial interests or personal relationships that could have appeared to influence the work reported in this paper.

Acknowledgements

The authors thank Bernhard Sartory and Konstantin Fischak, both from Materials Center Leoben (MCL) GmbH, Austria, for their work in preparing the APT specimens. The financial support by the Austrian Federal Ministry of Labour and Economy, the National Foundation for

Research, Technology and Development and the Christian Doppler Research Association is gratefully acknowledged. Transnational access to the ion beam analysis facility at Uppsala University has been supported by the RADIATE project under the Grant Agreement 824096 from the EU Research and Innovation program HORIZON 2020. Accelerator operation at Uppsala University has been supported by the Swedish research council VR-RFI (#2019-00191).

Supplementary materials

Supplementary material associated with this article can be found, in the online version, at doi:10.1016/j.ultramic.2025.114200.

Data availability

Data will be made available on request.

References

[1] H. Riedl, D. Holec, R. Rachbauer, P. Polcik, R. Hollerweger, J. Paulitsch, P. H. Mayrhofer, Phase stability, mechanical properties and thermal stability of Y alloyed Ti–Al–N coatings, Surf. Coat. Technol. 235 (2013) 174–180, https://doi.org/10.1016/J.SURFCOAT.2013.07.030.

[2] S. Vepřek, M.G.J. Veprek-Heijman, P. Karvankova, J. Prochazka, Different approaches to superhard coatings and nanocomposites, Thin Solid Films 476 (2005) 1–29, https://doi.org/10.1016/j.tsf.2004.10.053.

[3] N. Ariharan, C.G. Sriram, N. Radhika, S. Aswin, S. Haridas, A comprehensive review of vapour deposited coatings for cutting tools: properties and recent advances, Trans. Inst. Met. Finish. 100 (2022) 262–275, https://doi.org/10.1080/00202967.2022.2037343.

[4] S. PalDey, S.C. Deevi, Properties of single layer and gradient (Ti,Al)N coatings, Mater. Sci. Eng. A. 361 (2003) 1–8, https://doi.org/10.1016/S0921-5093(03)00473-8.

[5] Z. Wang, Z. He, F. Chen, C. Tian, U.V. Valiev, C. Zou, D. Fu, Effects of N2 partial pressure on microstructure and mechanical properties of cathodic arc deposited TiBN/TiAlSiN nano-multilayered coatings, Mater. Today Commun. 31 (2022) 103436, https://doi.org/10.1016/j.mtcomm.2022.103436.

[6] A.K. Krella, Degradation of protective PVD coatings, Handbook of materials Failure Analysis with case studies from the Chemicals, Concrete and Power industries, Butterworth-Heinemann (2016) 411–440, https://doi.org/10.1016/B978-0-08-100116-5.00016-8.

[7] H. Waldl, M. Tkadletz, C. Czettl, M. Pohler, N. Schalk, Influence of multilayer architecture on microstructure and fracture properties of arc evaporated TiAlTaN coatings, Surf. Coat. Technol. 433 (2022) 128098, https://doi.org/10.1016/J.SURFCOAT.2022.128098.

[8] F. Pei, Y.X. Xu, L. Chen, Y. Du, H.K. Zou, Structure, mechanical properties and thermal stability of Ti1-xSixN coatings, Ceram. Int. 44 (2018) 15503–15508, https://doi.org/10.1016/J.CERAMINT.2018.05.210.

[9] L. Chen, Y. Du, S.Q. Wang, A.J. Wang, H.H. Xu, Mechanical properties and microstructural evolution of TiN coatings alloyed with Al and Si, Mater. Sci. Eng. A. 502 (2009) 139–143, https://doi.org/10.1016/j.msea.2008.10.013.

[10] I. Milošev, H.H. Strehblow, B. Navinšek, XPS in the study of high-temperature oxidation of CrN and TiN hard coatings, Surf. Coat. Technol. 74–75 (1995) 897–902, https://doi.org/10.1016/0257-8972(95)08360-X.

[11] A. Flink, T. Larsson, J. Sjölén, L. Karlsson, L. Hultman, Influence of Si on the microstructure of arc evaporated (Ti,Si)N thin films; evidence for cubic solid solutions and their thermal stability, Surf. Coat. Technol. 200 (2005) 1535–1542, https://doi.org/10.1016/j.surfcoat.2005.08.096.

[12] N. Schalk, Y. Moritz, G. Kumar, D. Holec, C. Hugenschmidt, V. Vadimovitch, L. Mathes, M. Schiester, C. Saringer, C. Czettl, M. Pohler, C. Mitterer, M. Tkadletz, Nanocomposite versus solid solution formation in the TiSiN system, Acta Mater 275 (2024) 120063, https://doi.org/10.1016/J.ACTAMAT.2024.120063.

[13] S. Vepřek, S. Reiprich, A concept for the design of novel superhard coatings, Thin Solid Films 268 (1995) 64–71, https://doi.org/10.1016/0040-6090(95)06695-0.

[14] Y. Moritz, C. Saringer, M. Tkadletz, A. Stark, N. Schell, I. Letofsky-Papst, C. Czettl, M. Pohler, N. Schalk, Oxidation behavior of arc evaporated TiSiN coatings investigated by in-situ synchrotron X-ray diffraction and HR-STEM, Surf. Coat. Technol. 404 (2020) 126632, https://doi.org/10.1016/J.SURFCOAT.2020.126632.

[15] H. Du, R.E. Tressler, K.E. Spear, C.G. Pantano, Oxidation studies of crystalline CVD silicon nitride, J. Electrochem. Soc. 136 (1989) 1527, https://doi.org/10.1149/1.2096955.

[16] F. Kauffmann, G. Dehm, V. Schier, A. Schattke, T. Beck, S. Lang, E. Arzt, Microstructural size effects on the hardness of nanocrystalline TiN/amorphous-SiNx coatings prepared by magnetron sputtering, Thin Solid Films 473 (2005) 114–122, https://doi.org/10.1016/j.tsf.2004.08.080.

[17] F. Tang, B. Gault, S.P. Ringer, P. Martin, A. Bendavid, J.M. Cairney, Microstructural investigation of Ti–Si–N hard coatings, Scr. Mater. 63 (2010) 192–195, https://doi.org/10.1016/J.SCRIPTAMAT.2010.03.050.

[18] D.L.J. Engberg, L.J.S. Johnson, J. Jensen, M. Thuvander, L. Hultman, Resolving mass spectral overlaps in atom probe tomography by isotopic substitutions – case of TiSi15N, Ultramicroscopy 184 (2018) 51–60, https://doi.org/10.1016/J.ULTRAMIC.2017.08.004.

[19] A.J. London, D. Haley, M.P. Moody, Single-ion deconvolution of mass peak overlaps for atom probe microscopy, Microsc. Microanal. 23 (2017) 300–306, https://doi.org/10.1017/S1431927616012782.

[20] T. Kinno, K. Kitamoto, S. Takeno, M. Tomita, Laser-assisted atom probe tomography of 15 N-enriched nitride thin films for analysis of nitrogen distribution in silicon-based structure, Appl. Surf. Sci. 349 (2015) 89–92, https://doi.org/10.1016/j.apsusc.2015.04.200.

[21] D.L.J. Engberg, Atom Probe Tomography of TiSiN Thin Films, Linköping University, 2015, https://doi.org/10.3384/lic.diva-122724. PhD diss.

[22] F. Vaz, L. Rebouta, P. Goudeau, J. Pacaud, H. Garem, J.P. Rivière, A. Cavaleiro, E. Alves, Characterisation of Ti1−xSixNy nanocomposite films, Surf. Coat. Technol. 133–134 (2000) 307–313, https://doi.org/10.1016/S0257-8972(00)00947-6.

[23] M. Bartosik, R. Hahn, Z.L. Zhang, I. Ivanov, M. Arndt, P. Polcik, P.H. Mayrhofer, Fracture toughness of Ti-Si-N thin films, Int. J. Refract. Met. Hard Mater. 72 (2018) 78–82, https://doi.org/10.1016/J.IJRMHM.2017.12.015.

[24] M. Diserens, J. Patscheider, F. Lévy, Mechanical properties and oxidation resistance of nanocomposite TiN–SiNx physical-vapor-deposited thin films, Surf. Coat. Technol. 120–121 (1999) 158–165, https://doi.org/10.1016/S0257-8972(99)00481-8.

[25] P. Ström, D. Primetzhofer, Ion beam tools for nondestructive in-situ and in-operando composition analysis and modification of materials at the Tandem Laboratory in Uppsala, J. Instrum. 17 (2022) P04011, https://doi.org/10.1088/1748-0221/17/04/P04011.

[26] M.A. Sortica, V. Paneta, B. Bruckner, S. Lohmann, M. Hans, T. Nyberg, P. Bauer, D. Primetzhofer, Electronic energy-loss mechanisms for H, He, and Ne in TiN, Phys. Rev. A. 96 (2017) 032703, https://doi.org/10.1103/PHYSREVA.96.032703.

[27] M. Hans, M. Tkadletz, D. Primetzhofer, H. Waldl, M. Schiester, M. Bartosik, C. Czettl, N. Schalk, C. Mitterer, J.M. Schneider, Is it meaningful to quantify vacancy concentrations of nanolamellar (Ti,Al)N thin films based on laser-assisted atom probe data? Surf. Coat. Technol. 473 (2023) 130020 https://doi.org/10.1016/J.SURFCOAT.2023.130020.

[28] H. Waldl, M. Hans, M. Schiester, D. Primetzhofer, M. Burtscher, N. Schalk, M. Tkadletz, Decomposition of CrN induced by laser-assisted atom probe tomography, Ultramicroscopy 246 (2023) 113673, https://doi.org/10.1016/J.ULTRAMIC.2022.113673.

[29] M. Tkadletz, H. Waldl, M. Schiester, A. Lechner, G. Schusser, M. Krause, N. Schalk, Efficient preparation of microtip arrays for atom probe tomography using fs-laser processing, Ultramicroscopy 246 (2023) 113672, https://doi.org/10.1016/J.ULTRAMIC.2022.113672.

[30] M. Hans, J.M. Schneider, On the chemical composition of TiAlN thin films - comparison of ion beam analysis and laser-assisted atom probe tomography with varying laser pulse energy, Thin Solid Films 688 (2019) 137251, https://doi.org/10.1016/J.TSF.2019.04.026.

[31] L. Mancini, N. Amirifar, D. Shinde, I. Blum, M. Gilbert, A. Vella, F. Vurpillot, W. Lefebvre, R. Lardé, E. Talbot, P. Pareige, X. Portier, A. Ziani, C. Davesnne, C. Durand, J. Eymery, R. Butté, J.F. Carlin, N. Grandjean, L. Rigutti, Composition of wide bandgap semiconductor materials and nanostructures measured by atom probe tomography and its dependence on the surface electric field, J. Phys. Chem. C. 118 (2014) 24136–24151, https://doi.org/10.1021/JP5071264.

[32] D.R. Kingham, The post-ionization of field evaporated ions: a theoretical explanation of multiple charge states, Surf. Sci. 116 (1982) 273–301, https://doi.org/10.1016/0039-6028(82)90434-4.

[33] L. Tegg, L.T. Stephenson, J.M. Cairney, Estimation of the electric field in atom probe tomography experiments using charge state ratios, Microsc. Microanal. 30 (2024) 466–475, https://doi.org/10.1093/mam/ozae047.

[34] B. Gault, D.W. Saxey, M.W. Ashton, S.B. Sinnott, A.N. Chiaramonti, M.P. Moody, D. K. Schreiber, Behavior of molecules and molecular ions near a field emitter*, New J. Phys. 18 (2016) 033031, https://doi.org/10.1088/1367-2630/18/3/033031.

[35] O. Cojocaru-Mirédin, Y. Yu, J. Köttgen, T. Ghosh, C.-F. Schön, S. Han, C. Zhou, M. Zhu, M. Wuttig, Atom probe tomography: a local probe for chemical bonds in solids, Adv. Mater. 36 (2024) 2403046, https://doi.org/10.1002/ADMA.202403046.

[36] H. Holleck, V. Schier, Multilayer PVD coatings for wear protection, Surf. Coat. Technol. 76–77 (1995) 328–336, https://doi.org/10.1016/0257-8972(95)02555-3.

[37] H. Fager, J.M. Andersson, J. Jensen, J. Lu, L. Hultman, Thermal stability and mechanical properties of amorphous coatings in the Ti-B-Si-Al-N system grown by cathodic arc evaporation from TiB2, Ti33Al67, and Ti85Si15 cathodes, J. Vac. Sci. Technol. A. 32 (2014) 061508, https://doi.org/10.1116/1.4897170.

[38] M. Hans, J.M. Schneider, Electric field strength-dependent accuracy of TiAlN thin film composition measurements by laser-assisted atom probe tomography, New J. Phys. 22 (2020) 33036, https://doi.org/10.1088/1367-2630/ab7770.

[39] M. Schiester, H. Waldl, M. Hans, M. Thuvander, D. Primetzhofer, N. Schalk, M. Tkadletz, Influence of multiple detection events on compositional accuracy of TiN coatings in atom probe tomography, Surf. Coat. Technol. 477 (2024) 130318, https://doi.org/10.1016/J.SURFCOAT.2023.130318.

[40] N.E. Holden, T.B. Coplen, J.K. Böhlke, L.V. Tarbox, J. Benefield, J.R. de Laeter, P. G. Mahaffy, G. O'Connor, E. Roth, D.H. Tepper, IUPAC periodic table of the elements and isotopes (IPTEI) for the education community (IUPAC Technical Report), Pure Appl. Chem. 90 (2018) 1833–2092, https://doi.org/10.1515/pac-2015-0703.

[41] J.G. Brons, A.A. Herzing, K.T. Henry, I.M. Anderson, G.B. Thompson, Comparison of atom probe compositional fidelity across thin film interfaces, Thin Solid Films 551 (2014) 61–67, https://doi.org/10.1016/J.TSF.2013.11.105.
[42] D.J. Larson, T.J. Prosa, R.M. Ulfig, B.P. Geiser, T.F. Kelly, Local Electrode Atom Probe Tomography, 3rd ed., Springer Sci. New York, US, 2013.
[43] T.T. Tsong, Field ion image formation, Surf. Sci. 70 (1978) 211–233, https://doi.org/10.1016/0039-6028(78)90410-7.
[44] A. Bachmaier, H. Aboulfadl, M. Pfaff, F. Mücklich, C. Motz, Structural evolution and strain induced mixing in Cu–Co composites studied by transmission electron microscopy and atom probe tomography, Mater. Charact. 100 (2015) 178–191, https://doi.org/10.1016/J.MATCHAR.2014.12.022.